BIOCHEMISTRY
including biophysical chemistry & molecular biology
Article

Biochemistry **2010,** *49,* 9715–9721 9715
DOI: 10.1021/bi100877y

Discovery of Biphasic Thermal Unfolding of OmpC with Implications for Surface Loop Stability[†]

Neil Keegan,[‡] Helen Ridley,[§] and Jeremy H. Lakey*[,§]

[‡]*Institute of Cellular Medicine, Newcastle University, Newcastle Upon Tyne NE2 4HH, U.K., and* [§]*Institute for Cell and Molecular Biosciences, Newcastle University, Newcastle Upon Tyne NE2 4HH, U.K.*

Received June 1, 2010; Revised Manuscript Received October 7, 2010

ABSTRACT: *Escherichia coli* outer membrane protein C (osmoporin) is a close homologue of OmpF or matrix porin, expressed under conditions of high osmolarity or ionic strength. Despite the fact that the proteins display very similar structures (rmsd = 0.78 Å), the channel activities (gating or selectivity) of the two proteins are markedly different, and compared to OmpF, there is much less published information about the stability and folding of OmpC. In this paper, we report a structural study of nine OmpC mutations that affect channel size and voltage gating. The secondary and tertiary structural analysis by circular dichroism (CD) indicated that the single-amino acid substitutions have little impact on the protein fold. However, a thermal denaturation study using CD and differential scanning calorimetry shows that different mutations lead to varied levels of destabilization, with the largest showing a 15 °C lower T_m than the wild type and a 40% reduction in ΔH_{cal}. CD thermal denaturation measurements revealed that OmpC unfolds in a biphasic process, in which only the second phase is affected by the known mutations. The first stage of unfolding was shown to be reversible and separate from the main unfolding and loss of trimeric structure occurring in the second phase, leaving the flexible extracellular loops as the likely site of unfolding. The first phase is abolished as OmpC becomes more stable at lower pH.

The molecular sieve behavior of the outer membranes of Gram-negative bacteria is conferred by porin proteins spanning the lipid bilayer. Since their initial discovery by Nakae (*1*), a large porin superfamily has been classified and categorized as nonspecific or specific depending on the selectivity of their pores across a wide range of Gram-negative bacteria. The major porins in *Escherichia coli* K12, OmpF and OmpC,[1] are termed nonspecific, showing a linear relationship between solute concentration and translocation rate, allowing the passive diffusion of solutes of up to 600 and 500 Da, respectively (*2*). As OmpC (osmoporin) is upregulated at the expense of OmpF (matrix porin) under extreme environmental conditions, such as high osmolarity, it was believed that the physiological relevance of expressing the two proteins lay in a smaller physical size of the OmpC pore compared to OmpF (*3*). Planar lipid bilayer experiments supported this idea, demonstrating single-channel conductance values in 1 M NaCl of ~800 and ~500 pS for OmpF and OmpC, respectively (*4*−*6*). However, it is now known that single-channel conductance can be a poor measure of channel size because the charge distribution within the pore can clearly influence channel conductance (*7*). Finally, the crystal structures for *E. coli* OmpF, *Klebsiella pneumoniae* OmpK36 (OmpC homologue), and most recently *E. coli* OmpC itself revealed channel diameters that were virtually superimposable (*8*−*10*). In fact, the OmpF and OmpC crystal structures demonstrate 74% structural alignment of the pore-lining residues, showing an almost identical construction of the barrel core (*10*). The common feature is a constriction zone or eyelet in each pore, where acidic residues on loop 3 face basic residues on the barrel wall creating an electrostatic field unique to each protein. This distribution of ionizable residues in this eyelet region accounts nicely for the cation selectivities (P_{Na}/P_{Cl}) of OmpF and OmpC of 4 and 30, respectively (*4*, *8*, *11*). From a physical perspective, the crystal structures revealed that the main differences between OmpF and OmpC are in the extracellular loops, particularly a 14-residue insertion in loop 4 of OmpC. The role of electrostatic pore potential, in the physiological relevance of OmpF and OmpC, is still not resolved. Basle et al. (*10*) suggest that on the basis of the OmpC crystal structure an as yet unknown loop conformational change or long-distance modulation of pore potential must be considered.

The OmpC mutant proteins used in this study derive from pioneering work by Misra and Benson (*12*, *13*) . Using *E. coli* strain RAM105 (*OmpF*$^-$ *LamB*$^-$ *OmpC*$^+$ Tet^r), solely expressing OmpC in its outer membrane, they subjected it to a strong selective pressure on pore size by using maltodextrins as the sole carbon source. Analysis of those mutant colonies with a faster-growing phenotype revealed *ompC* mutations causing amino acid substitutions, small deletions and insertions, within a region now known to be within the eyelet (*10*). Growth tests, antibiotic sensitivities, and rates of ^{14}C uptake suggested enlargement of the pore, while a planar lipid bilayer study revealed that all the mutants exhibited increased conductance compared to that of wild-type (WT) OmpC (*5*). More surprisingly, these OmpC mutants acquired a voltage gating behavior characteristic of OmpF but absent from WT OmpC.

[†]This work was supported by a Medical Research Council Priority Area Studentship (G70/55) and the Biological and Biotechnological Research Council (BRIC BB/F005768/1).

*To whom correspondence should be addressed: Institute for Cell and Molecular Biosciences, University of Newcastle, Framlington Place, Newcastle NE2 4HH, U.K. Telephone: +441912228865. Fax: +441912227442. E-mail: j.h.lakey@ncl.ac.uk.

[1]Abbreviations: OmpC, outer membrane protein C; DSC, differential scanning calorimetry; CD, circular dichroism.

Published on Web 10/08/2010

Table 1: .OmpC Pore Mutants Studied Here[a]

OmpC protein	mutation position
WT	–
R37H	β-sheet 2
R74S	β-sheet 4
R74C	β-sheet 4
R74G	β-sheet 4
D105G	loop 3
R74RVA	β-sheet 4
ΔW103−F110	loop 3
R74RVA/D105G	β-sheet 4 and loop 3

[a]Five substitutions occurring at three different sites. A two-amino acid insertion, a large deletion, and a double additive mutant have undergone structural comparison.

An identical selection conducted with OmpF produced a homologous set of mutations at sites conserved in OmpC (*14*). These OmpF mutants have been subjected to extensive crystallographic and functional characterization (*15*, *16*). The crystallography demonstrated only small predictable changes in local structure demonstrating a maximum increase in pore size of 10% (*15*). However, functional analysis showed an increased rate of disaccharide uptake, dramatically different ion selectivity, and a reduced single-channel conductance (*16*). The reduced single-channel conductance is the opposite of that seen in the equivalent OmpC mutants (*5*). The results were validated by subsequent analysis of additional OmpF pore mutants, which demonstrated increased pore size with reduced conductance (*7*). This suggests that the unusual electrostatic field rather than physical size governs the ionic properties of the pore. From both structural and functional points of view, the OmpF literature is much more extensive, possibly because of the relatively recent availability of the OmpC X-ray structure (*10*). The OmpC pore mutations, which result in dramatically different functional consequences, have not been subjected to the same detailed structural analysis. In this paper, the Misra and Benson OmpC mutants that caused enlarged channels, increased permeability and voltage sensitivity, and lower protein stability were subjected to a detailed structural study, filling the gap in the literature compared to OmpF (*17*). Table 1 details the mutations studied, and Figure 1 displays their position within the OmpC three-dimensional crystal structure [Protein Data Bank (PDB) entry 2J1N]. Only one other OmpC pore mutant, a large deletion of loop 3, has undergone more detailed structural analysis (*18*). This mutant protein was shown to retain the majority of its secondary β-sheet structure but was less thermally stable than WT. In another study, site-directed mutagenesis of the *OmpC* gene produced a single-amino acid substitution (W56C) that demonstrated a reduced pore conductance (*19*).

The study allows, for the first time using circular dichroism spectroscopy (CD), fluorescence spectroscopy, and differential scanning calorimetry (DSC), a detailed comparison of the structural properties of WT OmpC, OmpF, and various mutant OmpC proteins with altered pore function. However, the study also revealed an entirely unexpected biphasic thermal unfolding in OmpC that is absent in OmpF. This was insensitive to destabilizing mutants in the pore, making surface loops likely areas for this initial unfolding.

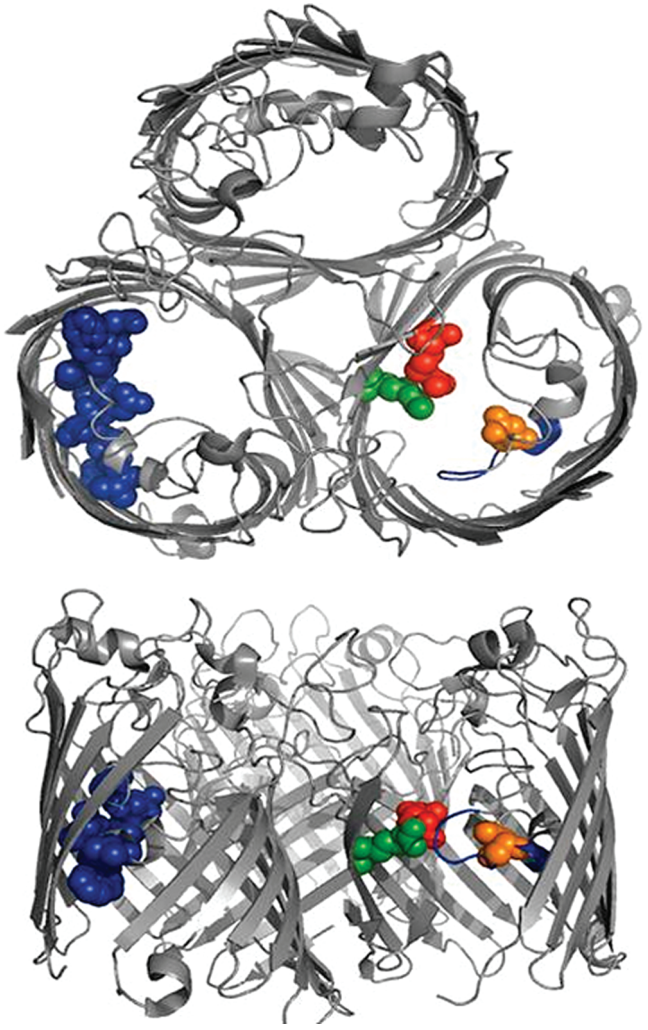

FIGURE 1: WT OmpC three-dimensional crystal structure (PDB entry 2J1N). OmpC mutants shown in colored space filling representation. In the top view, the uppermost extracellular loops are removed for the sake of clarity on two monomers of the trimer. The side view shows the extracellular face upward; the β-barrel has been cut away for the sake of clarity. R37 is colored green, R74 red, and D105 orange. W103−F110 are colored blue.

EXPERIMENTAL PROCEDURES

Materials. Prestained protein markers and bisacrylamide were obtained from Bio-Rad; SDS (sodium dodecyl sulfate), OGP (octyl β-D-glucopyranoside), and Octyl POE were from Melford laboratories. Tryptone, yeast extract, and bacterial agar were all obtained from Oxoid. Dialysis tubing was from Spectrum Laboratories Inc., and filters were purchased from Millipore or Sartorius. GE Healthcare supplied all the chromatography equipment with the exception of the Biospin 6 gel filtration columns (Bio-Rad). All other reagents were analytical grade and supplied by Sigma Chemical Co. and VWR International (BDH).

Protein Expression and Purification. Proteins were purified from bacterial strains constitutively expressing the desired gene. RAM105 (*OmpF*$^-$ *LamB*$^-$ *OmpC*$^+$ Tet^r) was used to express WT OmpC, while other strains derived from RAM105 were used to produce the OmpC mutants, namely, R74S (RAM120), R74insertionVA (RAM121), ΔW103−F110 (RAM122), R74G (RAM124), R74C (RAM270), R37H (RAM272), D106G (RAM280), and R74insertionVA and D105G (RAM363). Frozen glycerol stocks were used to seed LB

(Luria-Bertani) medium containing tetracycline at 10 μg/mL. Flasks were incubated at 37 °C in an orbital incubator at 180 rpm until the OD_{600} of the culture had reached a stationary phase of ~1.8, and cells were harvested by centrifugation at 6000 rpm for 15 min at 4 °C. Pelleted cells were resuspended in 20 mM phosphate buffer (pH 6.8) (15 mL/L of culture), supplemented with RNase A (10 μg/mL), DNase 1 (10 μg/mL), AEBSF (1 mM), and benzamidine (1 mM), followed by sonication in an ice bath (30 s on−off cycle for 10 min at a power setting of 14 microns) to break the cells. Cell debris was removed by centrifugation at 3000 rpm and 4 °C for 20 min, and the cell free supernatant was centrifuged at 40000 rpm for 1 h at 4 °C. The pellet, containing the membrane fraction, was washed and/or homogenized with 20 mM Tris (pH 7.4) and 2% SDS (10 mL/L of culture) at 55 °C for 1 h, followed by centrifugation as described in the previous step. Porin proteins were finally extracted from the washed membrane pellet by homogenization with 20 mM Tris, 2% SDS, and 0.5 M NaCl (pH 7.4) (10 mL/L of culture) at 37 °C for 1 h. The homogenate was centrifuged at 40000 rpm and room temperature for 1 h, leaving the extracted porin in the supernatant.

Further Purification and Buffer Exchange. Anion exchange chromatography was conducted on a 1 mL Hitrap DEAE Sepharose FF column and a GE Healthcare Akta*prime* system at a flow rate of 1 mL/min. The column was equilibrated with 10 column volumes of running buffer [1% Octyl POE and 20 mM Bis-Tris (pH 6.5)] before injection of the sample and washing with a further 10 column volumes of running buffer. Elution was achieved with a 0 to 0.5 M NaCl gradient. SDS−PAGE analysis was used to verify purity (Figure S1 of the Supporting Information). Further buffer exchange into the analysis buffers such as 1% OGP, 50 mM phosphate (pH 7.0), and acetate/borate buffers was conducted using dialysis tubing or gel filtration. All OmpC concentrations were assessed via UV−vis spectrophotometry using a WT extinction coefficient of 59880 M^{-1} cm^{-1} at 280 nm and an M_r of 38307. The typical protein yield was ~7.5 mg/L.

Spectroscopy and Calorimetry. All CD measurements were taken on a Jasco J-810 spectropolarimeter. A buffer baseline was subtracted from the protein spectrum for each experiment, the analysis buffer consisting of 1% OGP and 50 mM phosphate (pH 7.0). The samples were allowed to thermally equilibrate for 15 min prior to analysis. For far-UV CD spectra (180−250 nm), we used a 0.2 mm Hellma quartz cuvette, a 2 nm bandwidth, and a scan speed of 20 nm/min with a response time of 4 s, and the spectra were recorded as a minimum of five averaged accumulations, displayed as $\Delta\varepsilon$ (M^{-1} cm^{-1}) calculated using the mean residue concentration. For near-UV CD spectra (250−320 nm), we used the conditions described above except for a 1 cm Hellma quartz cuvette, and the spectra were displayed as $\Delta\varepsilon$ (M^{-1} cm^{-1}) calculated using the molar concentration of OmpC. Analysis of protein thermal unfolding followed the signal intensity at increasing temperatures at the wavelength of greatest change. For wavelengths of <250 nm, we used a Teflon-stoppered 1 mm Hellma quartz cuvette, while for wavelengths of >250 nm, we used a stoppered 10 mm cuvette. A heat ramp of 1 °C/min was applied and the CD monitored with a bandwidth of 5 nm, a response time of 32 s, and a data pitch of 1 °C. The buffer for thermal denaturation experiments was changed to acetate buffer ($\Delta pK_a\ K^{-1} = 0.0002$) for pH 5.0−5.5, phosphate ($\Delta pK_a\ K^{-1} = 0.0028$) for pH 5.8−7.5, and borate buffer ($\Delta pK_a\ K^{-1} = -0.008$) for pH 8.0−9.0 (*20*).

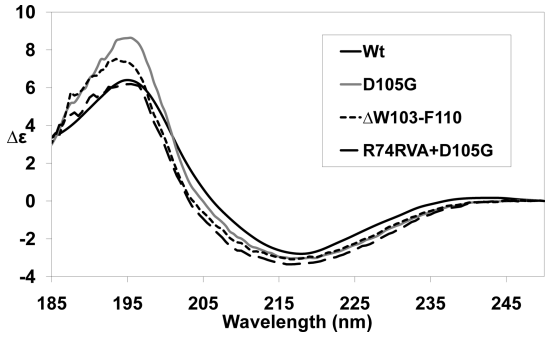

FIGURE 2: Far-UV CD spectra of WT and mutant OmpC proteins. The measurements were taken at 25 °C. Each spectrum is an average of five scans and has been corrected for the buffer baseline, a 0.2 mm light path, and the protein concentration on a mean residue basis. For conversion 1, ΔE (M^{-1} cm^{-1}) = 3300 deg cm^2 $dmol^{-1}$.

DSC experiments were performed using a MicroCal MCS, VP-DSC instrument. The protein sample was dialyzed several times against analysis buffer [1% OGP and 50 mM phosphate (pH 7.0)]. The final dialysis buffer was retained for use as a DSC reference and equilibration buffer. For the buffer baseline, both reference and sample cells were loaded with 0.512 mL of degassed buffer. Prior to the initiation of scanning, the pressure of the system was elevated to 30 psi and the thermostat equilibrated to the start temperature for 25 min. The buffer baselines were collected using a temperature range of 25−100 °C at a scan rate of 1 °C/min. After cooling, the sample cell was loaded with 0.512 mL of protein solution, and the scan was repeated using the same parameters. The data were processed using MicroCal Origin 7.0.

For fluorescence measurements, the protein was diluted to a concentration of 20 μg in 500 μL of 1% OGP and 50 mM phosphate (pH 7.0). The sample was added to a 5 mm path length Hellma cuvette and allowed to equilibrate to 25 °C within the sample chamber of a Cary Eclipse fluorescence spectrometer for 15 min. Using an excitation wavelength of 280 nm and excitation and emission slit widths of 5 nm, the emission spectrum was measured between 295 and 450 nm followed by subtraction of a blank buffer spectrum.

RESULTS AND DISCUSSION

Analysis of Secondary Structure. Far-UV CD was used to investigate the effect of each mutant on the secondary structure of OmpC. To remove NaCl and Octyl POE (which surprisingly showed a CD detectable phase change upon heating), all the protein solutions were dialyzed into 1% OGP and 50 mM phosphate (pH 7.0). Mutations located in the barrel wall have spectra largely identical to those of WT (Figure S2 of the Supporting Information). R37H has an enhanced signal at 196 nm, but because the intensities at 208 and 222 nm are unchanged, it could reflect an effect on Y35, which is in the proximity, rather than any helix formation. Tyrosines are known to absorb strongly at 195 nm with an ε_{max} of 50000 M^{-1} cm^{-1}, contributing to the far-UV signal of proteins more than anticipated in previous studies (*21*). Mutations located within loop 3 have slightly more pronounced deviations from WT spectra and are depicted in Figure 2. The negative maxima of all three mutants are more intense and shifted slightly (216−216.5 nm) compared to that of WT (218 nm). In addition, WT crosses zero at 206 nm, compared to D105G at 205 nm, ΔW103−F110 at 203.5 nm, and R74RVA/D105G at 203 nm. The spectra of WT

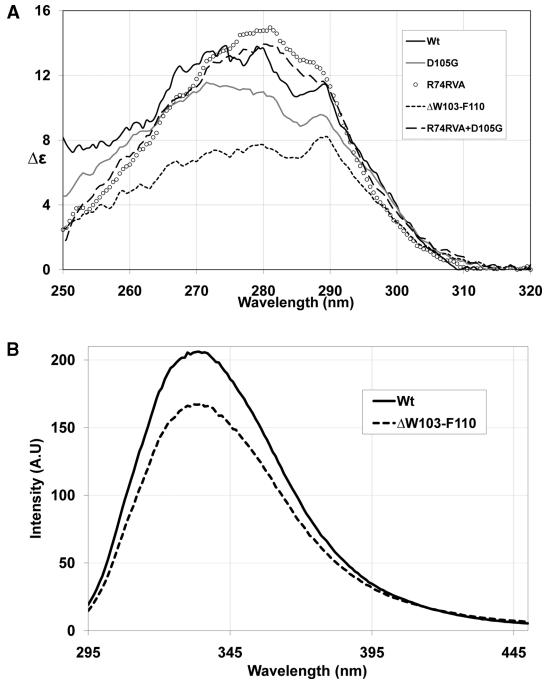

FIGURE 3: Tertiary structural analysis of WT and mutant OmpC proteins. (A) Near-UV CD spectra at 25 °C. Each spectrum is an average of five scans and has been corrected for the buffer baseline, a 10 mm light path, and the protein concentration expressed as protein molarity. (B) Fluorescence emission spectra of WT and ΔW103−F110. The proteins were diluted to 20 μg/mL, and measurements were taken at 25 °C with excitation of 280 nm. For conversion 1, ΔE (M^{-1} cm^{-1}) = 3300 deg cm^2 $dmol^{-1}$.

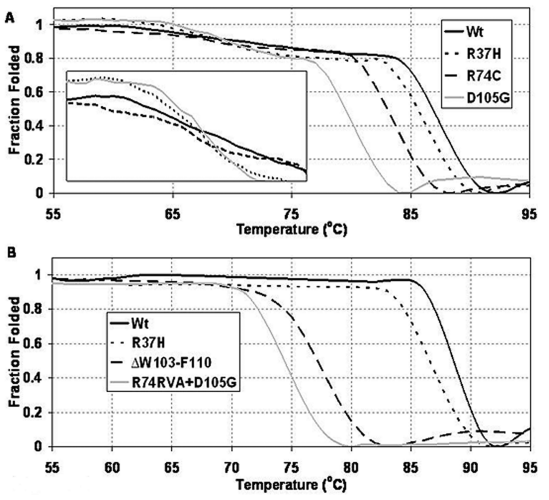

FIGURE 4: Thermal unfolding transitions of WT and mutant OmpC proteins. (A) Unfolding of four examples monitored by circular dichroism at 202 nm (secondary structure) while a heat ramp of 1 °C/min was applied to the sample. An exploded view of the initial transition can be seen in the inset. (B) Unfolding of four examples monitored by circular dichroism at 280 nm (tertiary structure) while a heat ramp of 1 °C/min was applied to the sample. The data for both panels have been normalized to 100% folded at the pretransition baseline and 0% folded in the post-transition region. Data for all the mutants are listed in Table 2.

and R74RVA/D105G demonstrate positive maxima and equal intensity around 196 nm, while the loop deletion (ΔW103−F110) and D105G show positive maxima with increased intensity. It again seems conceivable that tyrosines could be responsible for these changes in intensity, two being in the proximity of D105G and the loop deletion at positions 115 and 98. However, this aside, the differences in the mutant spectra from 230 to 200 nm are the most interpretable. The small deviations from WT spectra would suggest that the native β-barrel fold is maintained in each of the mutants.

Analysis of Tertiary Structure. Near-UV CD and fluorescence spectroscopy were used to investigate changes in tertiary structure. It is noteworthy that OmpF has a very weak near-UV CD spectrum (data not shown). OmpC is very different; near-UV results depicted in Figure 3A and Figure S3 of the Supporting Information demonstrate aromatic peaks across the entire spectrum. Large tryptophan peaks are present at 290 and 280 nm, and this peak then continues into the tyrosine absorption region and has still not dissipated when the phenylalanine absorption region is reached. The barrel interface of the tertiary fold is the most likely area of aromatic immobilization, in addition to constriction loop 3, which folds toward the barrel; both regions contain all three types of aromatic residues. The spectra for single-amino acid substitutions (R74S, R74C, R74G, and R37H) are virtually those of WT (Figure S3 of the Supporting Information). However, loop deletion ΔW103−F110 removes a tryptophan and a phenylalanine and results in a 44% signal loss at 280 nm (Figure 3A). Although it is an imperfect mutation for this reason, the large decrease in the magnitude of the signal is strong evidence that W103 contributes significantly to OmpC's near-UV CD signal. The likely source of the remaining signal is OmpC W252, which replaces F250 of OmpF. The signal of D105G also shows a decrease in the magnitude of the near-UV signal around 280 nm (Figure 3A), possibly related to the proximity of W103. The other proteins in Figure 3A are R74RVA and R74RVA/D105G. Their spectra are virtually superimposable, with a loss of the shoulder at 290 nm and a loss of the signal at 250 nm. This may be due to changes in either W72 within β-strand 4 or W56 in neighboring β-strand 3.

Only the deletion of W103−F110 causes a significant change in the fluorescence emission spectrum of OmpC, and because it results in a 19% reduction in emission intensity (Figure 3B), W103 appears to contribute less to OmpC fluorescence than it does to the near-UV CD signal. The fluorescence emission spectra of the other mutants resulted in the same λ_{max} as that of WT and an intensity within 5% of the WT value (Figure S4 of the Supporting Information). Overall, the mutations appear to provoke little change in the structure of OmpC and are similar to the equivalent OmpF mutations (*15*). It was previously shown by SDS−PAGE analysis that the OmpC mutants affect the thermal stability of the trimer (*5*), and this behavior was examined here in more detail.

Thermal Unfolding Analysis of OmpC. Porins are resistant to urea- or guanidine-induced denaturation, so the thermal unfolding was tested in a CD spectrometer. The proteins were all exposed to a heat ramp of 1 °C/min and the changes in secondary structure monitored at 202 nm. The tertiary structures for the two most and/or least heat stable OmpC proteins were subsequently measured at 280 nm. A complete set of far-UV CD spectra can be found in Figure S5 of the Supporting Information, and all demonstrate an unexpected biphasic unfolding. Thus, all the OmpC mutant proteins undergo an initial secondary structure unfolding above 55 °C, which ultimately removes approximately 10−20% of the CD signal (see Table 1, Figure 4A, and Figure S5 of the Supporting Information). This is followed by the main transition that is sensitive to the pore mutations (Table1). The pretransition is not observed in OmpF (data not shown). The

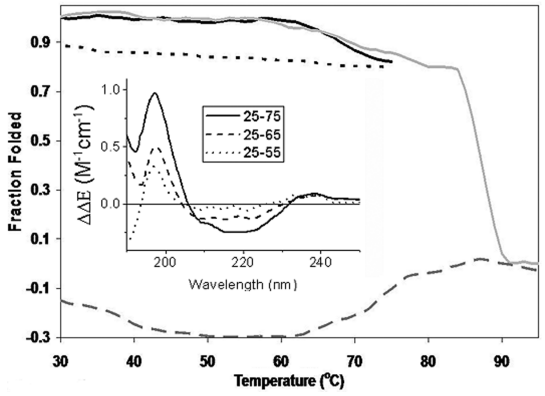

FIGURE 5: Thermal unfolding and refolding of WT OmpC. The main graph shows the circular dichroism of WT OmpC monitored at 202 nm while a heat increase or decrease (1 °C/min) was applied. The first scan (black) was cut short prior to the main unfolding transition and a reverse scan initiated immediately (black dashed line). At the end of the initial reverse scan, the protein was allowed a period of 2 h to regain structure before a second scan (gray) took the unfolding to completion. A reverse scan after full biphasic unfolding showed no sign of refolding on any time scale (gray dashed line). The inset shows the change in the full far-UV CD signal at 55, 65, and 75 °C after subtraction of the 25 °C data.

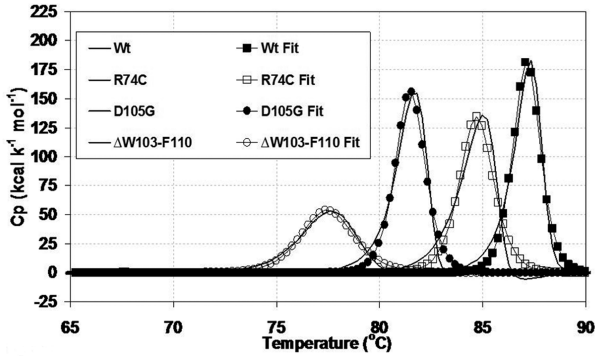

FIGURE 6: DSC thermograms for WT and mutant OmpC proteins. The proteins were scanned from 25 to 90 °C at a scan rate of 1 °C/min. The results have undergone standard processing; baseline subtraction, concentration normalization on a moles of monomer basis, and extrapolation of pre- and post-transition baselines using a linear progression. The best nonlinear least-squares approximation using a two-state $\Delta C_p = 0$ model of unfolding is shown for the four representative examples.

near-UV CD data (Figure 4B) show a single transition at the same time as the main secondary structure transition. This is likely to indicate that the trimer interface is lost at the same time as the main β-sheet secondary structure and is supported by the published SDS−PAGE analysis of trimer stability (*5*). The main denaturation transition is irreversible (Figure 5), which is expected because, for example, very specific conditions are required to refold OmpF from a urea-solubilized state (*27*). Thus, a true measure of thermodynamic stability is not possible. To test if the smaller initial unfolding step is reversible, the CD signal of WT OmpC was followed up to 75 °C, a point before the main unfolding step, and a reverse scan initiated. This showed no refolding during the 1 °C/min decrease in temperature to 25 °C. However, 2 h after this reverse scan, the protein was reanalyzed and showed the full biphasic OmpC denaturation signature (Figure 5). We were unable to obtain a reverse spectrum that showed no hysteresis, and this lack of true thermodynamic reversibility means that we cannot define the thermal stability of the first transition either. In a further experiment, a far-UV CD scan was measured at 25, 55, 65, and 75 °C, and the difference spectra that indicate the signal that has been lost have a minimum below 200 nm and cross the zero line at ~207 nm; this is most likely β-structure. This revealed that 10−20% of the β-fold is reversibly unfolded below 75 °C. The "loop" regions of porins are tightly packed, contain significant amounts of β-strand, and make up approximately 20% of the protein, so if these are involved in the first transition, retention of the core structure may provide a template for their refolding (*10*). Interestingly, the major structural differences between OmpF and OmpC are in the external loops, with loop 4 containing a 14-residue insert in OmpC that allows it to enhance the channel separation between monomers (*10*).

Complementary data were acquired via DSC (Figure 6 shows representative DSC data with a complete set in Figure S6 of the Supporting Information); DSC does not detect the initial unfolding possibly because it has a relatively small ΔH that is lost in the baseline subtraction step. A direct comparison of all the thermal transition data collected with the different techniques can be seen in Table 2. The agreement of each protein's T_m between techniques is excellent; WT is the most stable protein, as stable as R37H. Of the other single-amino acid substitutions, R74C is the most stable followed by three whose thermal unfolding is within a degree of each other (R74S, R74G, and D105G). The order of resistance to denaturation is very similar to the order of side chain bulk, which decreases (R > H > C > S > G) and also correlates with the changes in channel conductivity and gating (*5*). There is one further point; all the substitutions except histidine replace a charged amino acid with an uncharged one. As histidine could be partially protonated at pH 7, it may still fulfill the stabilizing role of the WT arginine, thus explaining the WT-like stability. The R74RVA barrel insertion is similar to three of the single-amino acid substitutions, which is slightly unexpected. Deletion ΔW103−F110 significantly reduces the size of constriction loop 3, which runs adjacent to the barrel wall, making a large number of stabilizing interactions; hence, the 11 °C destabilization of the protein is not so surprising. The highest degree of destabilization is shown by R74RVA/D105G, which demonstrates a 15 °C decrease in its T_m compared to that of WT. The factors destabilizing single entity mutations seem to be additive within this double mutation. The pore mutations, specifically D105G on loop 3, have a link to the evolution of antibiotic resistant bacteria, because a number of clinical isolates gain resistance to β-lactams through single-amino acid substitutions in porin proteins. The substitution of a small uncharged residue on loop 3 with a large charged residue, i.e., opposite of D105G, has resulted in antibiotic resistance in *Neisseria gonorrheae* and *Enterobacter aerogenes* (*22*−*24*). In addition, attachment of a fluorescent probe to R37C resulted in a stabilized mutant, so side chain size may correlate to stability rather than instability in the case of side chain reductions (*25*).

The results for the calorimetric enthalpy of unfolding ΔH_{cal} displayed in Table 2 are informative, but the absolute values should be treated with caution as protein unfolding should be reversible to give accurate thermodynamic information (*26*). R37H is the only mutant to show an increased ΔH_{cal} compared to that of WT. The mutations R74C, R74S, D105G, and R74RVA, which show a decrease in thermal stability, also demonstrate a reduction in ΔH_{cal} compared to that of WT. Surprisingly, R74G, with a lower thermal stability than WT, has a similar ΔH_{cal}, while ΔW103−F110 and R74RVA/D105G exhibit a greatly reduced ΔH_{cal}. Both of these larger mutations

Table 2: Summary of the Thermodynamic Parameters for WT and Mutant OmpC Unfolding[a]

	far-UV CD $T_m(1)$ (°C)	far-UV CD $T_m(2)$ (°C)	near-UV CD T_m (°C)	DSC T_m (°C)	DSC ΔH_{cal} (kcal/mol)
WT	69.9 ± 0.63	87.5 ± 0.04	88.5	86.97 ± 0.013	328 ± 3.69
R37H	68.4 ± 0.30	86.4 ± 0.05	86.5	87.28 ± 0.014	359 ± 4.67
R74C	68.4 ± 0.47	83.6 ± 0.04	−	84.62 ± 0.020	297 ± 4.91
R74S	68.1 ± 1.71	80.7 ± 0.05	−	81.71 ± 0.013	299 ± 3.75
R74RVA	68.7 ± 1.15	80.8 ± 0.05	−	81.31 ± 0.014	258 ± 3.45
R74G	68.1 ± 0.54	80.5 ± 0.04	−	80.78 ± 0.014	326 ± 4.21
D105G	69.5 ± 0.38	80.2 ± 0.05	−	81.53 ± 0.015	304 ± 4.02
ΔW103−F110	66.8 ± 2.35	75.9 ± 0.16	77.5	77.47 ± 0.025	184 ± 2.89
R74RVA/D105G	63.9 ± 0.62	72.5 ± 0.03	74.5	73.93 ± 0.030	192 ± 3.82

[a]We obtained the two transition temperatures [$T_m(1)$ and $T_m(2)$] from far-UV CD data collected using a 1 °C temperature ramp between 25 and 95 °C by fitting a four-parameter logistic (sigmoidal) function to each transition using a Marquardt−Levenberg nonlinear least-squares method and reporting the inflection point and its error as the T_m. For near-UV CD, we obtained the T_m by plotting the first-order derivative and obtaining the steepest slope. The uncertainty for DSC data is the standard deviation of the least-squares model fit to the data.

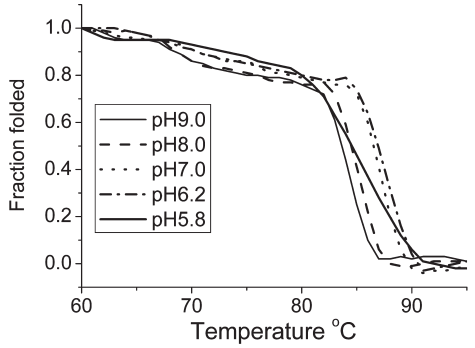

FIGURE 7: Effect of pH on the thermal stability of WT OmpC. Thermal denaturation was performed as described in the legend of Figure 4, except that OmpC samples were dialyzed into 1% OGP buffers at the indicated pH. Experiments at pH 5.0 showed no unfolding on this time scale, and the data are not plotted on these axes. Spectra taken 10 min after 95 °C had been reached revealed a reduction in secondary structure content (data not shown), indicating that unfolding does occur but does so more slowly than at higher pH values.

show a decrease in ΔH_{cal} of >40% compared to that of WT. In fact, a DSC study of OmpF revealed that single-amino acid substitutions, or a large deletion, in latching loop 2 produce large thermodynamic changes (*17*). Furthermore, Phale et al. also refer to DSC data for OmpF substitutions in the loop 3−barrel interface and a five-residue deletion in loop 3, stating they exhibited essentially WT behavior, not a trait demonstrated by their OmpC counterparts. The one OmpC pore mutant, a large deletion of loop 3, that has undergone prior DSC analysis validates our OmpC findings, demonstrating a 16 °C reduction in T_m compared to that of WT (*18*).

Effects of pH on Thermal Stability. The thermal stability (60−95 °C) of the OmpC WT protein was investigated over a range of pH values from 9.0 to 5.0. There is a trend toward greater thermal stability at lower pH, with a clear shift for the main transition from 85 to 87.5 °C between pH 8.0 and 7.0 (Figure 7). At pH 5.8, the main unfolding transition became shallow and the protein became so stable at pH 5.0 that it did not unfold during the experiment. The first phase of unfolding is clearest at high pH values, where the data resemble those of mutants R37H and D105G, and is effectively lost by pH 5.8. Extracellular loops contribute to pH sensitivity in OmpF (*27*), and this may explain the greater sensitivity to pH of the first phase of OmpC unfolding; however, clearly the whole molecule becomes very heat stable at low pH, an effect so far not observed in other porins.

Conclusions. Although the pore properties of the mutants in OmpF and OmpC are quite distinct, the secondary and tertiary structural changes caused by OmpC mutants are similar to those described in the X-ray crystallographic study of comparative OmpF mutants (*15*). The overall secondary and tertiary folds of the single-amino acid substitutions remain virtually unchanged from those of WT. However, the thermal denaturation study shows that although the overall protein fold may be maintained, different localized mutations lead to varied levels of destabilization in the protein as a whole. Thus, although the side chains point into a water-filled cavity, their mutant phenotypes resemble protein core, rather than surface, mutations (*28*). The study also revealed a voltage sensitive OmpC mutant (R37H) that exhibited a high level of stability and could be used as a sensitive nanoswitch within tethered lipid bilayer systems (*29*).

These studies led to the discovery of a reversible thermal unfolding transition, a characteristic so far unique to OmpC. It was insensitive to the destabilizing pore mutants, and the data implicate the outer loops in this reversible unfolding. A further study using known loop deletions could verify the site of the reversible changes, and methods such as AFM (*30*) and neutron reflectivity could show the degree of loop conformation changes (*29*, *31*).

ACKNOWLEDGMENT

We thank R. Misra and S. Benson for their generosity in providing OmpC strains for our work, Christopher Lakey for data analysis, and Arnaud Basle and James R. Henderson for critical reading of the manuscript.

SUPPORTING INFORMATION AVAILABLE

Complete data sets for all mutants and details of purification. This material is available free of charge via the Internet at http://pubs.acs.org.

REFERENCES

1. Nakae, T. (1976) Identification of the outer membrane protein of *E. coli* that produces transmembrane channels in reconstituted vesicle membranes. *Biochem. Biophys. Res. Commun. 71*, 877–884.
2. Nikaido, H., and Rosenberg, E. Y. (1983) Porin channels in *Escherichia coli*: Studies with liposomes reconstituted from purified proteins. *J. Bacteriol. 153*, 241–252.
3. Pratt, L. A., Hsing, W., Gibson, K. E., and Silhavy, T. J. (1996) From acids to osmZ: Multiple factors influence synthesis of the OmpF and OmpC porins in *Escherichia coli*. *Mol. Microbiol. 20*, 911–917.
4. Lakey, J. H., Watts, J. P., and Lea, E. J. (1985) Characterisation of channels induced in planar bilayer membranes by detergent solubilised *Escherichia coli* porins. *Biochim. Biophys. Acta 817*, 208–216.

5. Lakey, J. H., Lea, E. J., and Pattus, F. (1991) OmpC mutants which allow growth on maltodextrins show increased channel size and greater voltage sensitivity. *FEBS Lett. 278*, 31–34.
6. Buehler, L. K., Kusumoto, S., Zhang, H., and Rosenbusch, J. P. (1991) Plasticity of *Escherichia coli* porin channels. Dependence of their conductance on strain and lipid environment. *J. Biol. Chem. 266*, 24446–24450.
7. Phale, P. S., Philippsen, A., Widmer, C., Phale, V. P., Rosenbusch, J. P., and Schirmer, T. (2001) Role of charged residues at the OmpF porin channel constriction probed by mutagenesis and simulation. *Biochemistry 40*, 6319–6325.
8. Cowan, S. W., Schirmer, T., Rummel, G., Steiert, M., Ghosh, R., Pauptit, R. A., Jansonius, J. N., and Rosenbusch, J. P. (1992) Crystal structures explain functional properties of two *E. coli* porins. *Nature 358*, 727–733.
9. Dutzler, R., Rummel, G., Alberti, S., Hernandez-Alles, S., Phale, P., Rosenbusch, J., Benedi, V., and Schirmer, T. (1999) Crystal structure and functional characterization of OmpK36, the osmoporin of *Klebsiella pneumoniae*. *Struct. Folding Des. 7*, 425–434.
10. Baslé, A., Rummel, G., Storici, P., Rosenbusch, J. P., and Schirmer, T. (2006) Crystal structure of osmoporin OmpC from *E. coli* at 2.0 Å. *J. Mol. Biol. 362*, 933–942.
11. Karshikoff, A., Spassov, V., Cowan, S. W., Ladenstein, R., and Schirmer, T. (1994) Electrostatic properties of two porin channels from *Escherichia coli*. *J. Mol. Biol. 240*, 372–384.
12. Misra, R., and Benson, S. A. (1988) Genetic identification of the pore domain of the OmpC porin of *Escherichia coli* K-12. *J. Bacteriol. 170*, 3611–3617.
13. Misra, R., and Benson, S. A. (1988) Isolation and characterization of OmpC porin mutants with altered pore properties. *J. Bacteriol. 170*, 528–533.
14. Benson, S. A., Occi, J. L., and Sampson, B. A. (1988) Mutations that alter the pore function of the OmpF porin of *Escherichia coli* K12. *J. Mol. Biol. 203*, 961–970.
15. Lou, K. L., Saint, N., Prilipov, A., Rummel, G., Benson, S. A., Rosenbusch, J. P., and Schirmer, T. (1996) Structural and functional characterization of OmpF porin mutants selected for larger pore size. I. Crystallographic analysis. *J. Biol. Chem. 271*, 20669–20675.
16. Saint, N., Lou, K. L., Widmer, C., Luckey, M., Schirmer, T., and Rosenbusch, J. P. (1996) Structural and functional characterization of OmpF porin mutants selected for larger pore size. II. Functional characterization. *J. Biol. Chem. 271*, 20676–20680.
17. Phale, P. S., Philippsen, A., Kiefhaber, T., Koebnik, R., Phale, V. P., Schirmer, T., and Rosenbusch, J. P. (1998) Stability of trimeric OmpF porin: The contributions of the latching loop L2. *Biochemistry 37*, 15663–15670.
18. Rocque, W. J., and McGroarty, E. J. (1990) Structure and function of an OmpC deletion mutant porin from *Escherichia coli* K-12. *Biochemistry 29*, 5344–5351.
19. Bishop, N. D., Lea, E. J., Mobasheri, H., and Spiro, S. (1996) Altered voltage sensitivity of mutant OmpC porin channels. *FEBS Lett. 379*, 295–298.
20. Supelco (1995) Mobile Phases for Ion Exchange Chromatography and Chromatofocusing, Sigma-Aldrich.
21. Vuilleumier, S., Sancho, J., Loewenthal, R., and Fersht, A. R. (1993) Circular dichroism studies of barnase and its mutants: Characterization of the contribution of aromatic side chains. *Biochemistry 32*, 10303–10313.
22. Olesky, M., Hobbs, M., and Nicholas, R. A. (2002) Identification and analysis of amino acid mutations in porin IB that mediate intermediate-level resistance to penicillin and tetracycline in *Neisseria gonorrhoeae*. *Antimicrob. Agents Chemother. 46*, 2811–2820.
23. Gill, M. J., Simjee, S., Al-Hattawi, K., Robertson, B. D., Easmon, C. S., and Ison, C. A. (1998) Gonococcal resistance to β-lactams and tetracycline involves mutation in loop 3 of the porin encoded at the penB locus. *Antimicrob. Agents Chemother. 42*, 2799–2803.
24. De, E., Basle, A., Jaquinod, M., Saint, N., Mallea, M., Molle, G., and Pages, J. M. (2001) A new mechanism of antibiotic resistance in Enterobacteriaceae induced by a structural modification of the major porin. *Mol. Microbiol. 41*, 189–198.
25. Gokce, I., Bainbridge, G., and Lakey, J. H. (1997) Stabilising and destabilising modifications of cysteines in the *E. coli* outer membrane porin protein OmpC. *FEBS Lett. 411*, 201–205.
26. Hinz, H. J., and Schwarz, F. P. (2001) Measurement and analysis of results obtained on biological substances with differential scanning calorimetry. *Pure Appl. Chem. 73*, 745–759.
27. Basle, A., Qutub, R., Mehrazin, M., Wibbenmeyer, J., and Delcour, A. H. (2004) Deletions of single extracellular loops affect pH sensitivity, but not voltage dependence, of the *Escherichia coli* porin OmpF. *Protein Eng., Des. Sel. 17*, 665–672.
28. Baase, W. A., Liu, L. J., Tronrud, D. E., and Matthews, B. W. (2010) Lessons from the lysozyme of phage T4. *Protein Sci. 19*, 631–641.
29. Holt, S. A., Lakey, J. H., Daud, S. M., and Keegan, N. (2005) Neutron reflectometry of membrane protein assemblies at the solid/liquid Interface. *Aust. J. Chem. 58*, 674–677.
30. Cisneros, D. A., Muller, D. J., Daud, S. M., and Lakey, J. H. (2006) An approach to prepare membrane proteins forsingle-molecule imaging. *Angew. Chem., Int. Ed. 118*, 3330–3334.
31. Le Brun, A. P., Holt, S. A., Shah, D. S., Majkrzak, C. F., and Lakey, J. H. (2008) Monitoring the assembly of antibody-binding membrane protein arrays using polarised neutron reflection. *Eur. Biophys. J. 37*, 639–645.